Indian Journal of Chemical Technology
Vol. 32, November 2025, pp. 822-835
DOI: 10.56042/ijct.v32i6.14345

Entropy generation in chemically reactive pulsatile flow of Carreau-Yasuda nanofluid with Joule heating and thermal radiation: A Buongiorno model

J. Josuva & R. Hemadri Reddy[1]*

Department of Mathematics, School of Advanced Sciences, Vellore Institute of Technology, Vellore, Tamil Nadu, India

*E-mail: rhreddy@vit.ac.in

Received 12 October 2024; accepted 16 September 2025

This work provides a thermodynamic analysis of entropy-optimized heat and mass transfer in a Carreau-Yasuda nanofluid flow through a channel, with blood considered as the base fluid. It takes into account various factors, such as Brownian movement, thermophoresis, chemical reaction, thermal radiation, and viscous dissipation, with a particular emphasis on magnetohydrodynamic pulsating flow. Non-dimensional analysis facilitated the derivation of nonlinear dimensionless partial differential equations (PDEs), which were systematically reduced to ordinary differential equations (ODEs) using perturbation theory. The 'bvp4c' algorithm in MATLAB is then harnessed to produce the findings for the group of ODEs. The findings presented herein support the hypothesis that as the power law index, Hartmann number, and Carreau-Yasuda constant get higher, the velocity shrinks. Amplifying the Brownian motion, Eckert number, and thermophoresis parameters results in temperature surge. The concentration diminishes as thermophoresis, Lewis number, and chemical reaction rise, and it intensifies with larger levels of Brownian motion. Moreover, the rate of heat transmission is enhanced through improvements in the thermophoresis parameter and Weissenberg number, whereas contrasting features are noticed for the mass transfer rate at the bottom wall. Higher values of the Eckert number and Brownian motion parameter significantly proliferate entropy generation, while also causing Bejan number to diminish.

Keywords: Brownian motion, Carreau-Yasuda model, Chemical reaction, Entropy analysis, Pulsatile flow, Thermophoresis

Introduction

Extensive studies have been carried out on the thermal conductivity of nanofluids over the past three decades, building upon the revolutionary study of Choi[1]. Nanofluids, which consist of solid particles with sizes less than 100 nm stably suspended in a liquid base, are being used in a wide range of industries that require improved heat transfer. These industries include biosensors, food processing, nuclear power, mechanical engineering, and biomedicine[2,3]. Buongiorno[4] conducted an extensive investigation on nanofluids, examining the role of Brownian motion and thermophoretic dispersion of nanoparticles in enhancing thermal conductivity. Mahmoodi and Kandelousi[5] addressed entropy formation in nanofluid flow through a channel incorporating heat radiation, Brownian motion, and thermophoretic effects. Rajkumar *et al.*[6] analyzed chemically reactive micropolar nanofluid flow influenced by Brownian motion and thermophoretic diffusion. The heat transfer response of a tangent hyperbolic fluid around a sphere, influenced by Brownian motion and thermophoresis, was studied by Vedavathi *et al.*[7]. Anbuchezhian *et al.*[8] made use of Lie group operations to discover how the nanofluid boundary layer responds to thermal stratification caused by solar radiation. The consequences of temperature and solutal stratification on the unstable hydromagnetic flow of a nanofluid through the boundary layer on a flat surface was explored using Buongiorno's model by Mutuku and Makinde[9]. Madkhali *et al.*[10] explored the flow of a fluid containing three different types of nanoparticles between two expanding disks, utilising the finite element method.

Non-Newtonian fluids and their flow properties are attracting more and more scientific attention these days. Many different areas of science and industry can benefit from studying these special fluids, such as bio-medicine, oil recovery, coal slurries, food processing, petroleum drilling, and cosmetics. These fluids can be as different as blood, glue, honey, cream, perfume, and fuel. A special model called the Carreau-Yasuda model has proved to be useful in describing how these fluids get thinner or thicker when they flow. Particularly, it proves valuable in replicating non-Newtonian fluid behaviour, such as blood in physiology. Recent literature has presented classical

results. Khan *et al.*[11] discussed the impact of activation energy and chemical reaction on the flow of a magnetized Carreau-Yasuda fluid over a curved surface, aiming to minimize entropy generation. Qayyum *et al.*[12] adopted the methodology of homotopy analysis to inspect the unsteady flow of Carreau-Yasuda nanofluid (blood with nanoparticles) within a variable magnetic field. The analysis incorporated the effects of heat generation due to friction and the chemical reactions occurring within the fluid. Migtaa and Al-Khafajy[13] investigated the combined effects of heat and MHD on the flow of Carreau-Yasuda fluid, which thins out under shear stress, when moving across a permeable media. Dubey *et al.*[14] employed a finite element approach and the Carreau-Yasuda model to study heat transport in a bifurcated artery. Kada *et al.*[15] studied non-Newtonian fluid properties on the flow profile and transport efficiency generated by metachronal cilia waves in a 2D microsystem.

Pulsatile flow, distinguished by sinusoidally fluctuating pressure gradients in circular pipes/channels, has attracted considerable attention for its diverse applications in engineering, physiological processes and industrial fields. Its significance encompasses heat exchanger optimization, hydraulic pumps, blood flow in arterial networks, food processing design, respiratory and circulatory systems, MEMS manufacturing, cavitations in pipelines, and pressure surge analysis[16,17]. Radhakrishnamacharya and Maiti[18] examined energy transport rates in pulsating flow through a permeable channel. The consistent improvement in heat transmission over completely developed intermittent turbulent flow in a conduit was numerically demonstrated by Wang and Zhang[19].

Bhargava et al.[20] broke new ground by utilizing the finite element technique to scrutinize the pulsatile behavior of Casson fluid traversing through a Darcy-Forchheimer porous channel. Kumar and Prasad[21] examined the MHD pulsatile flow between permeable beds under homogeneous porous medium. Adesanya *et al.*[22] looked at how friction within a fluid affects its pulsating movement through a vertical porous channel. Govindarajulu *et al*[23]. employed a numerical approach to analyze the entropy generation within a third-grade fluid in a conduit with a pulsing flow. Thamizharasan and Reddy[24] investigated the interplay between thermophoresis, Brownian motion, Cattaneo-Christov heat flux, and magnetohydrodynamic pulsating flow on the behavior of Jeffrey nanofluid within a confined channel. Rajamani *et al.*[25] studied the flow behaviour of a couple-stress nanofluid under MHD pulsatile flow conditions within a channel incorporating Brownian motion and thermophoresis, and found that both effects increase heat transfer. Josuva and Reddy[26] performed a Buongiorno model-based analysis of pulsatile Carreau-Yasuda nanofluid flow with nonlinear radiation through an inclined porous channel. Similar studies on pulsatile flow can be found in the literature for Oldroyd-B nanofluid[27], Casson nanofluid[28], and Powell-Eyring Nanofluid[29].

Along with viscous dissipation and first-order chemical reactions, there is ample scope for studying thermal radiation, considering its practical implications in the fields of science and engineering, such as combustion studies, chemical reactor designs, polymer processes, solar energy systems, energy storage systems, electronics cooling, materials processing, and environmental modeling. Hayat *et al.*[30] figured out that an elevation in thermal radiation contributes to a decrease in temperature across the boundary layer for an upper-convected Maxwell fluid within a permeable conduit. Sheikholeslami *et al.*[31] found that increasing the radiation parameter enhances the heat transfer rate in nanofluid flow between rotating parallel plates under a magnetic field. Ibrahim and Negera[32] as well as Pal and Talukdar[33] analyzed the effects of thermal radiation, chemical reaction, and joule heating on unsteady flow using computational techniques; the former studied a Williamson nanofluid over a stretching/shrinking wedge, while the latter researched was an endlessly moving vertical porous plate. Daniel *et al.*[34] discovered that the combination of radiation and magnetic field in conjunction with chemical reaction limits the concentration of nanoparticles across stretched sheet. Balla and Naikoti[35] numerically studied Newtonian fluid flow over an infinitely long vertical plate, incorporating thermal radiation, viscous dissipation, and a first-order chemical reaction.

A detailed survey of the existing literature reveals that the effects of thermophoresis, viscous dissipation, Brownian motion, Joule heating, and thermal radiation on the MHD pulsatile transport of Carreau-Yasuda nanofluid in a channel configuration have not been investigated. Thus, this study aims to bridge the existing research gap by providing an in-depth examination of this neglected phenomenon, thereby contributing insights applicable to biomedical fluid

transport, clinical therapeutics, vitamin delivery systems, dialysis procedures, and industrial flow processes. Through the perturbation process, the complexities of the governing PDEs are reduced to a tractable system of ODEs, allowing for efficient numerical analysis. Subsequent solving is carried out using the bvp4c package in MATLAB, with support from the shooting technique. The temperature, velocity, and concentration of the nanofluid are visually represented using numerical data. A detailed tabulation of the heat and mass transport rates is provided.

Mathematical modeling

Flow pattern

We undertook this study to examine the behaviour of nanofluid, based on the Carreau-Yasuda model that has been subjected to electrical treatment in a channel exhibiting laminar and incompressible pulsatile flow conditions. The adopted flow domain is illustrated in Fig. 1. Cartesian coordinate system has been acknowledged as a convenient approach for the scrutiny of fluid flow by orienting the x^*-axis parallel to the lower surface and the y^*-axis orthogonal to it. The distance h, separates the top and bottom walls.The temperature, velocity, and concentration of the fluid are all considered to be functions of the x^*-coordinate. Additionally, it is also known that the only non-zero velocity component is the one in the x^*-direction, which is represented by u^*. For fully developed flow, the axial velocity gradient vanishes, i.e., $\frac{\partial u^*}{\partial x^*} = 0$. As a result, the continuity equation shows that $\frac{\partial v^*}{\partial y^*} = 0$, which indicates the transverse velocity v^*remains constant along the channel height and is zero at the channel boundaries. The y^*-momentum equation is represented as $\frac{\partial P^*}{\partial y^*} = 0$ [29,36]

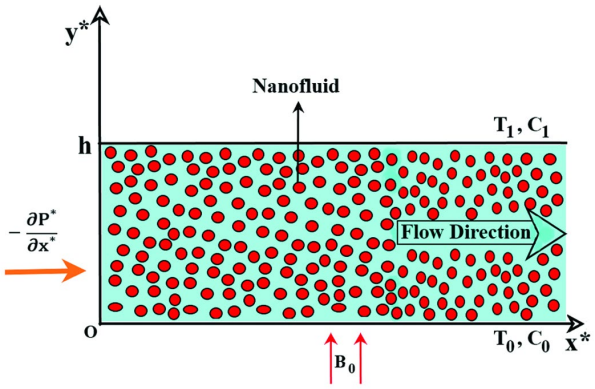

Fig. 1 — Schematic of current flow pattern

representing a critical component of the fluid dynamics of the system.

This research uses the Buongiorno concept to ascertain the correlation between thermophoresis and Brownian movement. The entire study encompasses variables associated with viscous dissipation, chemical reaction, Joule heating, and thermal radiation. A uniform magnetic field, denoted as B_0, consistently permeates the walls and the induced magnetic field is intentionally disregarded. The temperatures at the upper and lower walls, denoted as T_1 and T_0 accordingly, satisfy the condition that T_0 is lower than T_1. Similarly, the concentrations of nanoparticles at the upper and lower walls, denoted as C_1 and C_0 correspondingly, it must satisfy the criterion that C_0 is less than C_1.

Carreau-Yasuda rheological model

The Carreau-Yasuda constitutive equation takes the form[13,14,15]:

$$S = -PI + [\mu_\infty + (\mu_0 - \mu_\infty)(1 + (\Gamma\dot{\gamma})^d)^{\frac{n-1}{d}}]A_1, \ldots(1)$$

In this context, P denotes the pressure, μ_∞ signifies the viscosity at infinite shear rate, I stands as the identity tensor, while Γ, d, and n serve as parameters characterizing the Carreau-Yasuda fluid. The term μ_0 denotes the viscosity at zero shear rate, and A_1 corresponds to the first Rivlin-Ericksen tensor, where the shear rate is stated as $\dot{\gamma} == \sqrt{\frac{1}{2}\mathrm{tr}(A_1^2)}$, with $A_1 = [\nabla V + (\nabla V)^T]$. Moreover, μ_∞ is thought to be negligibly small, leading to the modified form of Eq. …(1) as follows:

$$S = -PI + [\mu_0(1 + (\Gamma\dot{\gamma})^d)^{\frac{n-1}{d}}]A_1, \quad \ldots(2)$$

The fluid exhibits the characteristics of shear thinning (pseudoplastic) when $n < 1$, and shear thickening (dilatant) when $n > 1$. If the exponent $\Gamma = 0$ and/or $n = 1$, the fluid displays Newtonian behavior. Our focus in this study will be on exploring non-Newtonian behavior.

Formulation of the problem

The flow problem is governed by equations elucidating the dynamics of momentum, energy, and concentration, as provided below [12,23,25,26]:

$$\frac{\partial u^*}{\partial t^*} = -\frac{1}{\rho_f}\frac{\partial P^*}{\partial x^*} + \frac{\mu_f}{\rho_f}\frac{\partial^2 u^*}{\partial y^{*2}} + \frac{\mu_f}{\rho_f}\left(\frac{n-1}{d}\right)\Gamma^d(d + 1)\left(\frac{\partial u^*}{\partial y^*}\right)^d\frac{\partial^2 u^*}{\partial y^{*2}} - \frac{\sigma_f}{\rho_f}B_0^2 u^*, \quad \ldots(3)$$

$$\frac{\partial T^*}{\partial t^*} = \frac{k_f}{(\rho C_p)_f}\frac{\partial^2 T^*}{\partial y^{*2}} + \frac{\mu_f}{(\rho C_p)_f}\left(\frac{\partial u^*}{\partial y^*}\right)^2 + \frac{\mu_f}{(\rho C_p)_f}\Gamma^d\left(\frac{n-1}{d}\right)\left(\frac{\partial u^*}{\partial y^*}\right)^2\left(\frac{\partial u^*}{\partial y^*}\right)^d - \frac{1}{(\rho C_p)_f}\frac{\partial q_r}{\partial y^*} + \frac{\sigma_f}{(\rho C_p)_f}B_0^2 u^{*2} + \tau\left[D_B\left(\frac{\partial C^*}{\partial y^*}\frac{\partial T^*}{\partial y^*}\right) + \frac{D_T}{T_m}\left(\frac{\partial T^*}{\partial y^*}\right)^2\right], \quad \ldots(4)$$

$$\frac{\partial C*}{\partial t^*} = D_B\frac{\partial^2 C^*}{\partial y^{*2}} + \frac{D_T}{T_m}\frac{\partial^2 T^*}{\partial y^{*2}} - k_1 C^*. \quad \ldots(5)$$

The symbol u^* stands for the x^*-direction velocity; the density and viscosity of fluidare denoted by ρ_f and μ_f; its electrical and thermal conductivities by σ_f and k_f; and its effective specific heat by $(\rho C_p)_f$. The variables T^* and C^* denote the temperature and concentration of nanoparticle, respectively. q_r is the radiative heat flux, and $\tau = (\rho C_p)_p/(\rho C_p)_f$, where $(\rho C_p)_p$ is the effective heat capacity of nanoparticle. The respective diffusion coefficients for thermophoresis and Brownian motion are symbolized by D_T and D_B. The first-order chemical reaction is represented by k_1, and the mean temperature is T_m.

The conditions at the boundary(B.Cs):

$$u^*(0) = 0, T^*(0) = T_0, C^*(0) = C_0 \quad \ldots(6)$$

$$u^*(h) = 0, T^*(h) = T_1, C^*(h) = C_1 \quad \ldots(7)$$

Applying the Rosseland approximation results in the simplification of the radiative heat flux (q_r)as follows[34,36]:

$$q_r = -\left(\frac{4\sigma^*}{3\kappa^*}\right)\frac{\partial T^{*4}}{\partial y^*} \quad \ldots(8)$$

where the Rosseland mean absorption coefficient is $\kappa^*$and the Stefan-Boltzmann constant is σ^*. When the temperature variations inside the fluid are negligible enough, T^{*4} can be represented as a function of temperature. The truncated Taylor series expansion of T^{*4} about T_1 is:

$$T^{*4} = 4T^*T_1^3 - 3T_1^3 \quad \ldots(9)$$

Utilizing the aforementioned Eqs. …(8) and …(9), Eq. …(4) transformed into:

$$\frac{\partial T^*}{\partial t^*} = \frac{k_f}{(\rho C_p)_f}\frac{\partial^2 T^*}{\partial y^{*2}} + \frac{1}{(\rho C_p)_f}\frac{16\sigma^* T_1^3}{3\kappa^*}\frac{\partial^2 T^*}{\partial y^{*2}} + \frac{\mu_f}{(\rho C_p)_f}\left(\frac{\partial u^*}{\partial y^*}\right)^2 + \frac{\mu_f}{(\rho C_p)_f}\left(\frac{n-1}{d}\right)\Gamma^d\left(\frac{\partial u^*}{\partial y^*}\right)^2\left(\frac{\partial u^*}{\partial y^*}\right)^d + \frac{\sigma_f}{(\rho C_p)_f}B_0^2 u^{*2} + \tau\left[D_B\left(\frac{\partial C^*}{\partial y^*}\frac{\partial T^*}{\partial y^*}\right) + \frac{D_T}{T_m}\left(\frac{\partial T^*}{\partial y^*}\right)^2\right] \quad \ldots(10)$$

Now, introducing the subsequent set of dimensionless variables and parameters,

$$P = \frac{hP^*}{\mu_f U}, u = \frac{u^*}{U}, t = t^*\omega, y = \frac{y^*}{h}, x = \frac{x^*}{h}, \theta = \frac{T^*-T_0}{T_1-T_0}, \phi = \frac{C^*-C_0}{C_1-C_0}. \quad \ldots(11)$$

By employing Eq. …(11), Eqs. …(3), …(5), and …(10)were transformed into

$$H^2\frac{\partial u}{\partial t} = -\frac{\partial P}{\partial x} + \frac{\partial^2 u}{\partial y^2} + (We)^d\left(\frac{n-1}{d}\right)(d+1)\left(\frac{\partial u}{\partial y}\right)^d\frac{\partial^2 u}{\partial y^2} - M^2 u, \quad \ldots(12)$$

$$H^2\frac{\partial \theta}{\partial t} = \left(1+\frac{4}{3}Rd\right)\frac{1}{Pr}\frac{\partial^2\theta}{\partial y^2} + Ec\left(\frac{\partial u}{\partial y}\right)^2 + Ec(We)^d\left(\frac{n-1}{d}\right)\left(\frac{\partial u}{\partial y}\right)^2\left(\frac{\partial u}{\partial y}\right)^d + Nb\frac{\partial\theta}{\partial y}\frac{\partial\phi}{\partial y} + Nt\left(\frac{\partial\theta}{\partial y}\right)^2 + M^2 Ecu^2, \quad \ldots(13)$$

$$H^2\frac{\partial\phi}{\partial t} = \frac{1}{PrLe}\frac{\partial^2\phi}{\partial y^2} - \gamma_1\phi + \frac{1}{PrLe}\left(\frac{Nt}{Nb}\right)\frac{\partial^2\theta}{\partial y^2} - K_1. \quad \ldots(14)$$

where ω is the frequency, $H = \sqrt{\frac{\omega h^2}{\nu_f}}$ is frequency parameter, $M = B_0 h\sqrt{\frac{\sigma_f}{\mu_f}}$ is Hartmann number, $\gamma_1 = \frac{k_1 h^2}{\nu_f}$ is chemical reaction parameter, $Rd = \frac{4\sigma^* T_1^3}{\kappa^* k_f}$ is the radiation parameter, $Ec = \frac{U^2}{(C_p)_f(T_1-T_0)}$ is the Eckert number, $Pr = \frac{(\mu C_p)_f}{k_f}$ is Prandtl number, $Nb = \frac{\tau D_B(C_1-C_0)}{\nu_f}$ is Brownian motion parameter, $We = \frac{\Gamma U}{h}$ is Weissenberg number, $Nt = \frac{\tau D_T(T_1-T_0)}{T_m\nu_f}$ is the thermophoresis variable, $K_1 = \frac{k_1 C_0 h^2}{\nu_f(C_1-C_0)}$ is constant, $Le = \frac{k_f}{D_B(\rho C_p)_f}$ is Lewis number, and U is the characteristic velocity.

The non-dimensional B.Cs are

$$u(0) = 0, \quad \theta(0) = 0, \quad \phi(0) = 0, \quad \ldots(15)$$

$$u(1) = 0, \quad \theta(1) = 1, \quad \phi(1) = 1 \quad \ldots(16)$$

Solution of the problem

Acknowledging the pressure gradient as the driving factor for the flow, we approach the dimensionless pressure gradient in the following manner[21,30]:

$$-\frac{\partial P}{\partial x} = \lambda_0 + \epsilon\lambda_1 e^{it}. \quad \ldots(17)$$

Here λ_0 and λ_1 represent the frequencies of pulsatile component oscillations. The following expressions for *u,ϕ, and* θ originated from the formulation provided in Eq. …(17):

$$u(y,t) = u_0 + \epsilon u_1 e^{it}, \quad \ldots(18)$$

$$\phi(y,t) = \phi_0 + \epsilon \phi_1 e^{it}, \quad \ldots(19)$$

$$\theta(y,t) = \theta_0 + \epsilon \theta_1 e^{it}. \quad \ldots(20)$$

By substituting Eqs (17)-(20) into Eqs (12) -(14), the coefficients of ϵ for powers up to and including one can be isolated for each power, resulting in the following set of ODEs:

$$u_0'' + (We)^d \left(\frac{n-1}{d}\right)(d+1)(u_0')^d u_0'' - M^2 u_0 + \lambda_0 = 0, \quad \ldots(21)$$

$$u_1'' + \left(\frac{n-1}{d}\right)(d+1)(We)^d (u_0')^d u_1'' + (We)^d (d+1)(n-1)(u_0')^{d-1} u_0'' u_1' - (M^2 + iH^2)u_1 + \lambda_1 = 0, \quad \ldots(22)$$

$$\left(1+\frac{4}{3}Rd\right)\frac{1}{Pr}\theta_0'' + Ec(u_0')^2 + Ec\left(\frac{n-1}{d}\right)(We)^d (u_0')^2 (u_0')^d + Nb\theta_0'\phi_0' + Nt(\theta_0')^2 + EcM^2 u_0^2 = 0, \quad \ldots(23)$$

$$\left(1+\frac{4}{3}Rd\right)\frac{1}{Pr}\theta_1'' + Ec\left(\frac{n-1}{d}\right)(We)^d \left(d(u_0')^{d-1}(u_0')^2 u_1' + 2u_0'(u_0')^d u_1'\right) + 2Ecu_0'u_1' + Nb\theta_1'\phi_0' + 2Nt\theta_0'\theta_1' + Nb\theta_0'\phi_1' + 2EcM^2 u_0 u_1 - i\theta_1 H^2 = 0, \quad \ldots(24)$$

$$\frac{1}{Pr}\phi_0'' + \frac{1}{Pr}\left(\frac{Nt}{Nb}\right)\theta_0'' - Le\gamma_1\phi_0 - LeK_1 = 0, \quad \ldots(25)$$

$$\frac{1}{Pr}\phi_1'' + \frac{1}{Pr}\left(\frac{Nt}{Nb}\right)\theta_1'' - Le(\gamma_1 + iH^2)\phi_1 = 0. \quad \ldots(26)$$

The primes indicate differentiation concerning the variable y.

The established B.Cs:

$$u_0 = 0, u_1 = 0, \theta_0 = 0, \theta_1 = 0, \phi_0 = 0, \phi_1 = 0 \; at \; y = 0, \quad \ldots(27)$$

$$u_0 = 0, u_1 = 0, \theta_0 = 1, \theta_1 = 0, \phi_0 = 1, \phi_1 = 0 \; at \; y = 1. \quad \ldots(28)$$

Moreover, at the boundary, Nusselt and Sherwood numbers, referring to non-dimensional heat and mass transfer rates, are defined as follows[23,26]:

$$Nu = \left(1+\frac{4}{3}Rd\right)\left[\frac{d\theta_0}{dy} + \epsilon e^{it}\frac{d\theta_1}{dy}\right]_{y=0,1} \quad \ldots(29)$$

$$Sh = \left[\frac{d\phi_0}{dy} + \epsilon e^{it}\frac{d\phi_1}{dy}\right]_{y=0,1} \quad \ldots(30)$$

Numerical scheme

Taking advantage of MATLAB's bvp4c solver with shooting scheme, we efficiently compute numerical solutions for nonlinear reduced higher-order boundary value problems (BVPs). This method, renowned for its speed and accuracy, leverages the Runge-Kutta fourth-order method. It also optimizes initial guesses using the Newton-Raphson algorithm to ensure precise solutions. Fig. 2 offers an in-depth overview of the 'bvp4c' algorithm.

First-order ordinary differential equations (ODEs) have been created from the nonlinear ODEs given in Eqs (21)-(26). These ODEs are presented as follows:

$$z_2' = \left(\frac{d}{d+(We)^d(n-1)(d+1){z_2}^d}\right)(M^2 z_1 - \lambda_0), \quad \ldots(31)$$

$$z_4' = \left(\frac{d}{d+(We)^d(n-1)(d+1)z_2{}^d}\right)(-(d+1)(We)^d(n-1){z_2}^{d-1}z_2' z_4 + (M^2+iH^2)z_3 - \lambda_1), \quad \ldots(32)$$

$$z_6' = \left(\frac{-3Pr}{3+4Rd}\right)(Ec{z_2}^2 + Ec\left(\frac{n-1}{d}\right)(We)^d {z_2}^2 z_2{}^d + Nbz_6 z_{10} + Nt{z_6}^2 + EcM^2{z_1}^2), \quad \ldots(33)$$

$$z_8' = \left(\frac{-3Pr}{3+4Rd}\right)(2Ecz_2 z_4 + Ec\left(\frac{n-1}{d}\right)(We)^d\left(d{z_2}^{d-1}{z_2}^2 z_4 + 2z_2 z_2{}^d z_4\right) + Nb(z_8 z_{10} + z_6 z_{12}) + 2Ntz_6 z_8 + 2EcM^2 z_1 z_3 - iH^2 z_7), \quad \ldots(34)$$

$$z_{10}' = -\left(\frac{Nt}{Nb}\right)z_6' + \gamma_1 PrLe z_9 + K_1 PrLe, \quad \ldots(35)$$

$$z_{12}' = -\left(\frac{Nt}{Nb}\right)z_8' + (\gamma_1 + iH^2)PrLe z_{11}. \quad \ldots(36)$$

Here, $z_1 = u_0, z_2 = u_0', z_3 = u_1, z_4 = u_1', z_5 = \theta_0, z_6 = \theta_0', z_7 = \theta_1, z_8 = \theta_1', z_9 = \phi_0, z_{10} = \phi_0', z_{11} = \phi_1, z_{12} = \phi_1'$.

The defined boundary conditions:

$$z_1(0) = 0, z_3(0) = 0, z_5(0) = 0, z_7(0) = 0, z_9(0) = 0, z_{11}(0) = 0 \quad \ldots(37)$$

$$z_1(1) = 0, z_3(1) = 0, z_5(1) = 1, z_7(1) = 0, z_9(1) = 1, z_{11}(1) = 0 \quad \ldots(38)$$

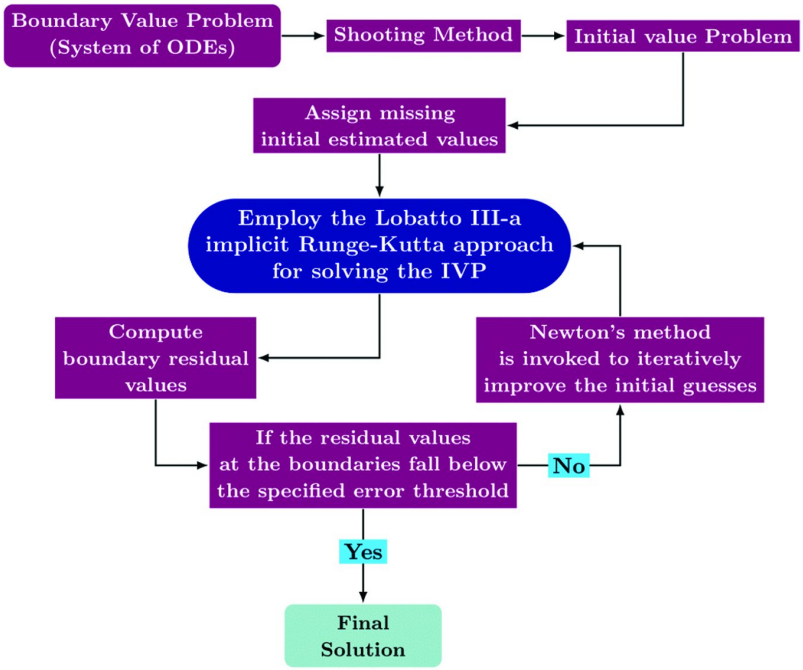

Fig. 2 — Flow diagram illustrating the numerical solution process

The above simplified equations (Eqs (31)-(36)) are analyzed for variable variations on subsequent profiles through numerical solutions employing the built-in *bvp4c* solver in MATLAB.

To verify the reliability of the numerical results obtained using the *bvp4c* method, comparative solutions were generated via the *dsolve* package in MAPLE 2024, configured with the *numeric* option. Additionally, the *bvp[traprich]* sub-method, which integrates the trapezoidal rule with Richardson extrapolation, was employed to enhance computational accuracy. The findings show that the tabulated metrics from these two distinct software programs have a high degree of concordance, as evidenced by Table 1.

Entropy Generation

In the case of Carreau-Yasuda nanofluid within a channel, the dimensional form of the entropy generation (EG) equation is expressed as follows[11,23,25]:

$$EG = \frac{k_f}{T_0^2}\left[1+\frac{16\sigma^* T_1^3}{3\kappa^* k_f}\right]\left(\frac{\partial T^*}{\partial y^*}\right)^2 + \frac{R_g D}{C_0}\left(\frac{\partial C^*}{\partial y^*}\right)^2 + \frac{\mu_f}{T_0}\Gamma^d\left(\frac{n-1}{d}\right)\left(\frac{\partial u^*}{\partial y^*}\right)^2\left(\frac{\partial u^*}{\partial y^*}\right)^d + \frac{\sigma_f B_0^2}{T_0}u^{*2} + \frac{\mu_f}{T_0}\left(\frac{\partial u^*}{\partial y^*}\right)^2 + \frac{R_g D}{T_0}\frac{\partial C^*}{\partial y^*}\frac{\partial T^*}{\partial y^*} \quad \ldots(39)$$

The non-dimensional representation of entropy generation is

$$NG = \left(1+\frac{4}{3}Rd\right)\left(\frac{\partial\theta}{\partial y}\right)^2 + \frac{PrEc}{\Delta}\left(\frac{n-1}{d}\right)(We)^d\left(\frac{\partial u}{\partial y}\right)^2\left(\frac{\partial u}{\partial y}\right)^d + \frac{PrEc}{\Delta}\left(\frac{\partial u}{\partial y}\right)^2 + \frac{L}{\Delta}\frac{\partial\theta}{\partial y}\frac{\partial\phi}{\partial y} + \frac{EcPrM^2}{\Delta}u^2 + \frac{L\Lambda}{\Delta^2}\left(\frac{\partial\phi}{\partial y}\right)^2 \quad \ldots(40)$$

where, R_g is gas constant, D is diffusion term, NG $= \frac{EG}{EG_0}$, $EG_0\left(=\frac{k_f(T_1-T_0)^2}{T_0^2h^2}\right)$, $\Lambda\left(=\frac{C_1-C_0}{C_0}\right)$ the concentration difference, $\Delta\left(=\frac{T_1-T_0}{T_0}\right)$ the temperature difference, and $L\left(=\frac{R_gD(C_1-C_0)}{k_f}\right)$ the diffusivity parameter. We define the Bejan number (Be) as:

$$Be = \frac{\frac{L\partial\theta\partial\phi}{\Delta\partial y\partial y}+\left(1+\frac{4}{3}Rd\right)\left(\frac{\partial\theta}{\partial y}\right)^2+\frac{LY}{\Delta^2}\left(\frac{\partial\phi}{\partial y}\right)^2}{NG} \quad \ldots(41)$$

Results and Discussion

In this section, the flow dynamics of a pulsatile Carreau–Yasuda nanofluid exhibiting shear-thinning behavior (n < 1) are systematically investigated with respect to variations in key physical parameters, and the corresponding results are elucidated through detailed graphical illustrations and numerical data. Many physical parameters relevant to our model equations are discussed in detail, such as the Eckert

Table 1 — Evaluation of the present findings in comparison to those produced by dsolve for Nu and Sh at the upper wall when $We = 3, n = 0.5, d = 2, t = \frac{\pi}{4}, \epsilon = 0.1, Pr = 21, M = 0.3, Nb = 0.2, Le = 2.1, K_1 = 0.001, Rd = 2, \gamma_1 = 0.2, H = 1, Nt = 0.3, Ec = 2, \lambda_0 = 0.3,$ and $\lambda_1 = 0.2$

Parameters	Numerals	$(\mathrm{Nu})_{y=1}$		$(\mathrm{Sh})_{y=1}$	
		bvp4c	dsolve	bvp4c	dsolve
	3	0.43726874	0.43726691	3.67846076	3.67846119
Ec	3.5	0.40736575	0.40736568	3.68684441	3.68684442
	4	0.37743992	0.37743987	3.69523477	3.69523478
	0.2	0.72442604	0.72442601	3.44301933	3.44301934
Nt	0.3	0.49699601	0.49699576	3.66171599	3.66171605
	0.4	0.32781712	0.32781620	3.86349767	3.86349801
	0.2	0.49699601	0.49699576	3.66171599	3.66171605
Nb	0.3	0.27614855	0.27614845	3.45873759	3.45873761
	0.4	0.13974392	0.13974370	3.34645411	3.34645417
	1	0.02492102	0.02491747	3.65726004	3.65726142
Rd	1.5	0.21623859	0.21623780	3.67052306	3.67052332
	2	0.49699601	0.49699576	3.66171599	3.66171605

number (Ec), thermophoresis parameter (Nt), frequency parameter (H), chemical reaction parameter (γ_1), power-law index (n), Weissenberg number (We), Lewis number (Le), Brownian motion parameter (Nb), radiation parameter (Rd), Hartmann number (M), and Carreau-Yasuda constant (d).

The model incorporates the following dimensionless parameter values, which were referenced from the literature[11,12,23,26]:$M = 0.3, n = 0.5, H = 2, We = 3.0, Nb = 0.2, \lambda_0 = 0.3,\ \lambda_1 = 0.2, Pr = 21, Nt = 0.3, Ec = 2, \gamma_1 = 0.2, d = 2.0, Rd = 2, Le = 2.1, = 0.1, L = 0.001, \Delta = 0.2, \Lambda = 0.2, t = \frac{\pi}{3}$ and $K_1 = 0.001$. These values are considered constant, unless otherwise specified.

Velocity profile

Figs 3(a)-(d) present graphical insights of the alterations in steady velocity (u_s) concerning various parameters, such as n, d, We, and M. In Fig. 3(a), it is noticeable that an elevation in 'n' contributes to a decline in the system's steady velocity. The dimensionless parameter d shown in Fig. 3(b) indicates the boundary that divides the power-law area and zero shear rate, wherein an augmentation of the Carreau-Yasuda constant exhibits a reduction in the speed of fluid motion. Fig. 3(c) highlights the Weissenberg number's relationship with steady velocity, indicating that higher Weissenberg numbers contribute to an increase in steady velocity. This relationship is attributed to viscosity, as less viscous liquids tend to exhibit higher velocities. Finally, Fig 3(d) demonstrates the deceleration of steady velocity with an elevation in M, due to the elevated magnetic force in the fluid flow.

Figs 4(a)-(f) have been constructed to elucidate the impact of distinct parameters, including the Weissenberg number (We), power-law index (n), Hartmann number (M), Carreau-Yasuda constant (d), frequency parameter (H), and time (t), on the unsteady velocity (u_t). In Figs 4(a) and 4(b), a visual depiction of the fluid variables 'n' and 'd' is presented, revealing a monotonic decay in both u_t profiles as the values of these fluid variables increase. The influence of the We, which represents an improvement in unsteady velocity with a growing viscosity ratio parameter, gets easier to comprehend in Fig. 4(c). Fig. 4(d) illustrates a decrease in the unsteady velocity of Carreau-Yasuda nanoliquid as the quantities of M increase, which is explained by Lorentz forces produced from the magnetic field that is utilized. Furthermore, Fig. 4(e) indicates that as the frequency parameter goes up, the amplitude of oscillations becomes stronger, provoking a retardation of the unsteady velocity. Finally, the impression of t on unsteady velocity is showcased in Fig. 4 (f), demonstrating oscillatory behaviour with varying values of time.

Temperature profile

The significance of distinct physical variables - Brownian motion parameter (Nb), Eckert number (Ec), radiation parameter (Rd), and thermophoresis variable (Nt), about the steady temperature *(θ_s)* illustrated in Figs 5(a)-(d). Upon inspection of Fig. 5(a), one may confidently assert that augmentation in Rd weakens the constant temperature. The correlation arises from a general reduction in thermal boundary layer density, which leads to a corresponding decline

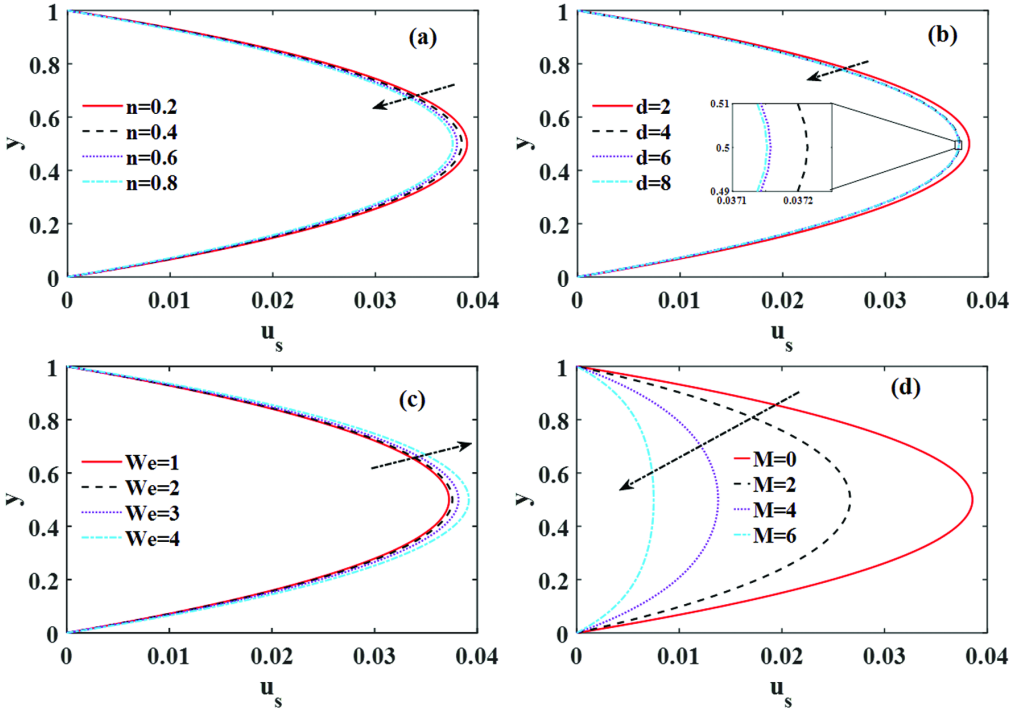

Fig. 3 — Response of steady velocity (u_s) to (a) n, (b) d, (c) We and (d) M

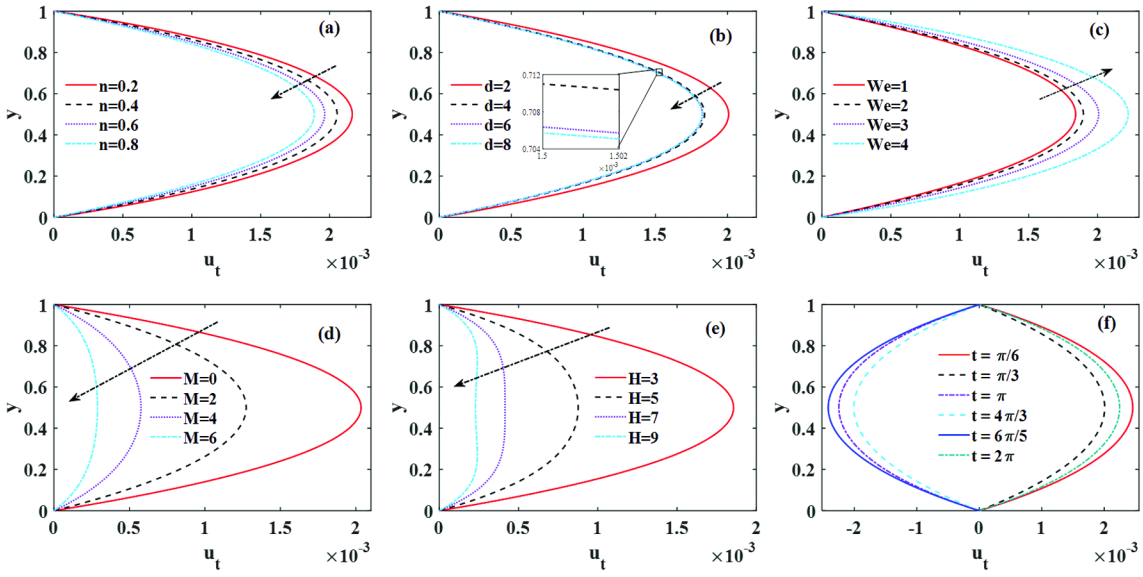

Fig. 4 — Response of unsteady velocity (u_t) to (a) n, (b) d, (c) We, (d) M, (e) H and (f) t

in θ_s. The adverse effect of Ec is evident in Fig. 5(b), demonstrating an upsurge in steady temperature with increasing Ec. This phenomenon is attributed to heightened viscous dissipation, i.e., generating more heat due to increased friction between particles and molecular movement. Both Figs 5(c) and 5(d) illustrates increasing steady temperature profile as Nt along with Nb increases. This phenomenon may be explained by the fact that particles made of colloidal material move more unpredictably as a consequence of enhanced Brownian movement and stronger fluid particle transmission brought about by enhanced thermophoresis, which boosts the θ_s.

Figs 6(a)-(f) highlight how different parameters, such as n, d, Rd, Ec, We, Nt, M, Nb, and t, exert influence on the nanofluid's unsteady temperature (θ_t). Fig. 6(a) depicts the fluctuating nature of unsteady temperature at strengthening Rd values. The

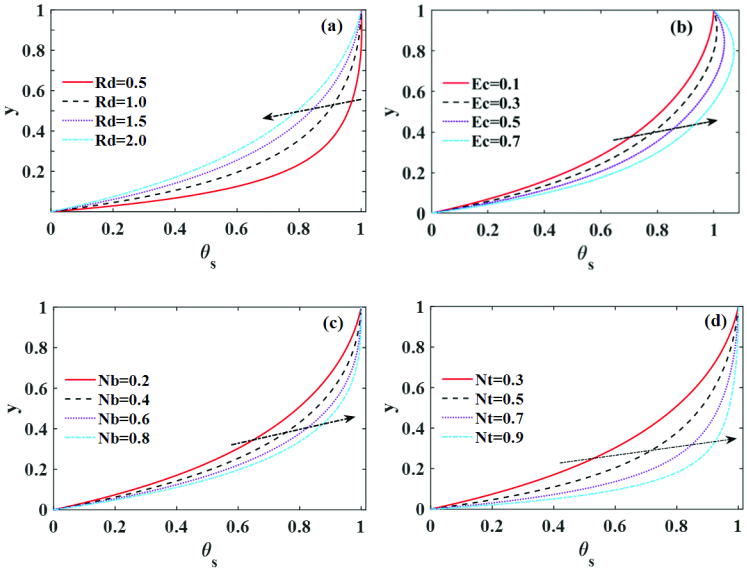

Fig. 5 — Response of steady temperature (θ_s) to (a) Rd, (b) Ec, (c) Nb and (d)Nt

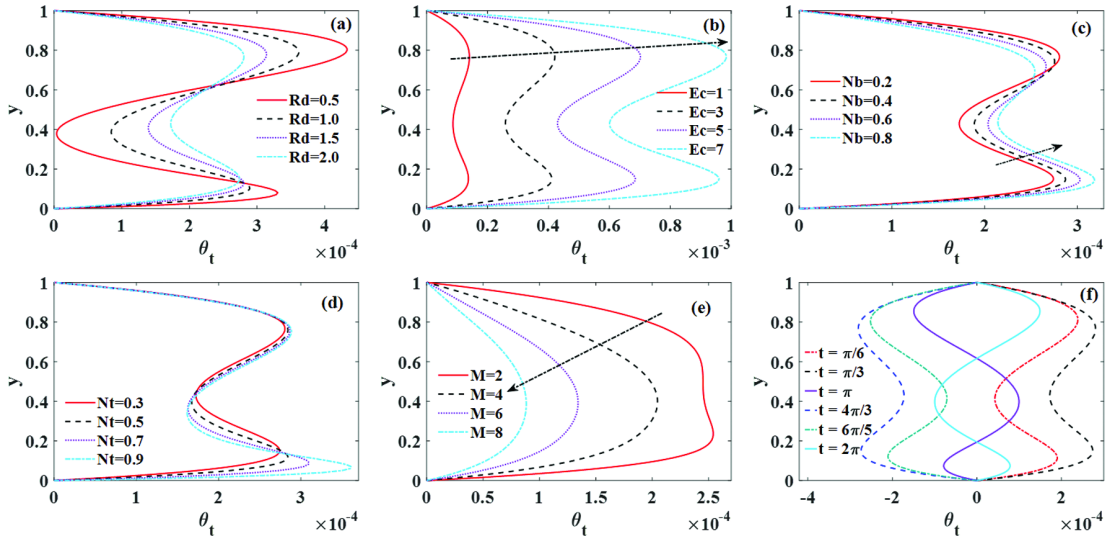

Fig. 6 — Response of unsteady temperature (θ_t) to (a) Rd, (b) Ec, (c) Nb, (d) Nt, (e) M and (f) t

correlation between the Ec and θ_t is visualized in Fig. 6(b), indicating that an elevated Ec hastens the nanofluid temperature, reaching its maximum near both the top and lower walls. Figs 6(c) and 6(d) demonstrate the fluctuating character of unsteady temperature, attributed to the acceleration of Nb coupled with Nt. This effect is induced by the chaotic motion of nanoparticles at the point closest to the bottom wall where the temperature is highest. An upturn in magnetic parameter is tied to a downturn in unsteady temperature, as outlined in Fig. 6(e). Finally, the oscillating pattern of an unsteady temperature emerging with distinct t values can be recognized in Fig. 6(f).

Concentration profile

The consequences of the wide-ranged parameter settings of thermophoresis variable (Nt), chemical reaction parameter (γ_1), Lewis number (Le), and Brownian movement (Nb) against the steady concentration distribution (ϕ_s) are portrayed in Figs 7(a)-(d). As seen from Fig. 7(a), there is a discernible relationship between decrease in ϕ_s and rise in Nt. On the other hand, when the levels of Nb increase, opposite trends become noticeable, especially regarding steady concentration. This phenomenon is attributed to the stochastic motion of particles, which allows them to disperse throughout the fluid domain and amplifies a steady concentration

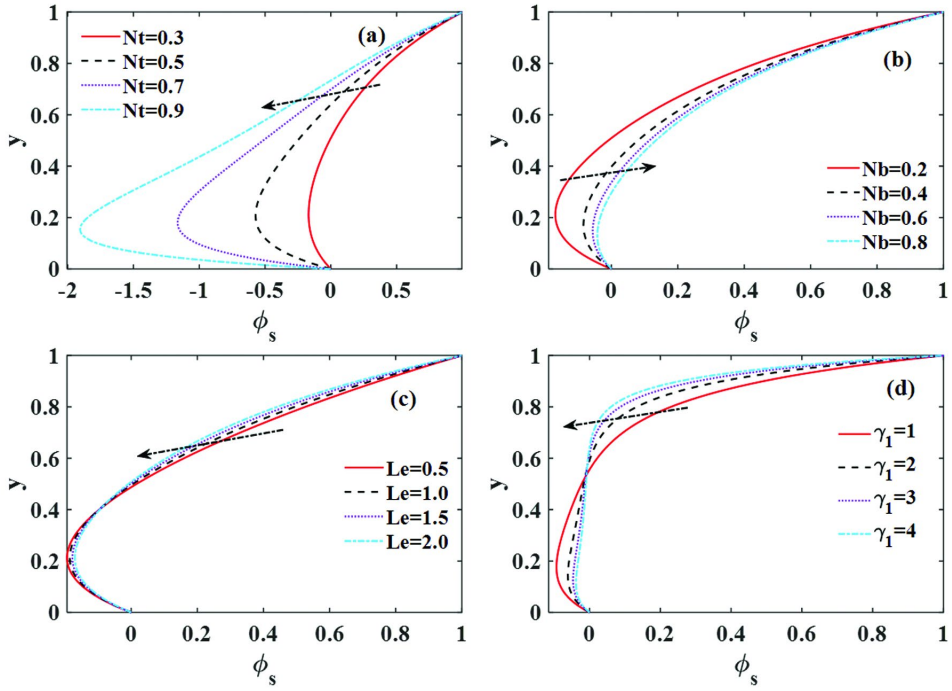

Fig. 7 — Response of steady concentration (ϕ_s) to (a) Nt, (b) Nb, (c) Le and (d) γ_1

(Ref. Fig. 7(b)). Fig. 7(c) reveals a deceleration in ϕ_s as Lewis number values increase, indicating improved mass transfer rates for higher Le values, subsequently reducing nanoparticle concentration. Escalating γ_1 shows similar mannerisms concerning steady concentration, as depicted in Fig. 7(d).

The profiles of unsteady concentration (ϕ_t) are portrayed in Figs 8(a)-(d), highlighting the ramifications of Nt, Le, γ_1, and Nb. Figs 8(a) and 8(b) elucidate the fluctuation in ϕ_t corresponding to variations in Nt and Nb. Showcasing the outcomes associated with changes in Le and γ_1 displayed in Figs 8(c) and 8(d) concerning ϕ_t, both spotlighting an oscillating nature of unsteady concentration for incrementing Le and γ_1, respectively.

Entropy generation

Figs 9(a)-(e) shed light on how entropy generation (NG) is affected by the Eckert number (Ec), radiation parameter (Rd), Hartmann number (M), Brownian motion parameter (Nb), and diffusion variable (L). The graph in Fig. 9(a) demonstrates that entropy generation rises with enhanced Ec values, a result of kinetic energy outweighing the enthalpy difference. The magnetic field's interaction with the fluid flow induces a Lorentz force, resulting in a diminution in NG in the vicinity of the walls, as demonstrated in Fig. 9 (b). An enhancement in entropy generation is observed in Fig. 9(c) and 9(d) with the improvement in Rd and L values. The enhanced thermal conductivity of nnaofluid drives the uptick in NG with an elevation in Rd. In the same way, faster nanoparticle diffusion within the system boosts entropy generation as L expands. Fig. 9 (e) reveals that NG rises near the lower wall but falls near the upper wall as the Brownian motion parameter grows. This pattern is a result of random movement of the nanoparticles in the fluid.

Bejan number

The impact of Eckert number (Ec), Brownian motion parameter (Nb), radiation parameter (Rd), Hartmann number (M), and diffusion variable (L) on Bejan number (Be) is demonstrated in Figs 10(a)-(e). Fig. 10(a) illustrates the correlation between Ec and Be. As Ec increases, the viscous force intensifies, impacting fluid motion and subsequently lowering the Bejan number. Fig. 10(b) depicts the delaying force from the magnetic field as a key factor in raising the Bejan number when M increases. This behaviour is similarly observed with the radiation parameter in Fig. 10(c). According to Fig. 10(d), a surge in Be was connected to the disordered behavior of fast particle diffusion as the diffusion parameter grew. Fig. 10(e) illustrates that Be diminishes as the Brownian motion parameter grows, due to the heightened friction and heat generated from the chaotic movement of nanoparticles.

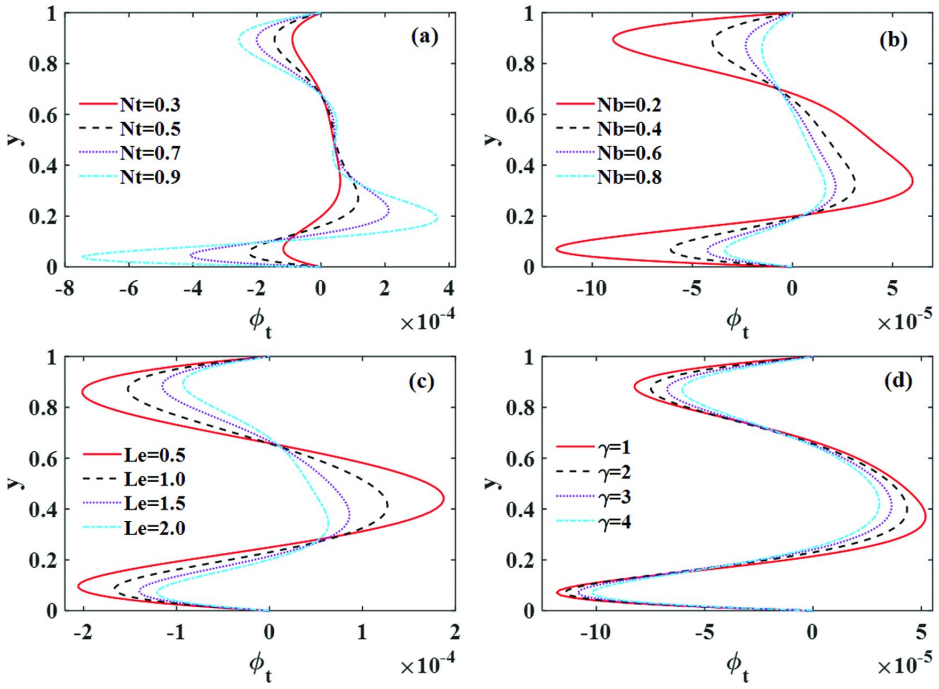

Fig. 8 — Response of unsteady concentration (ϕ_t) to (a) Nt, (b) Nb, (c) Le and (d) γ_1

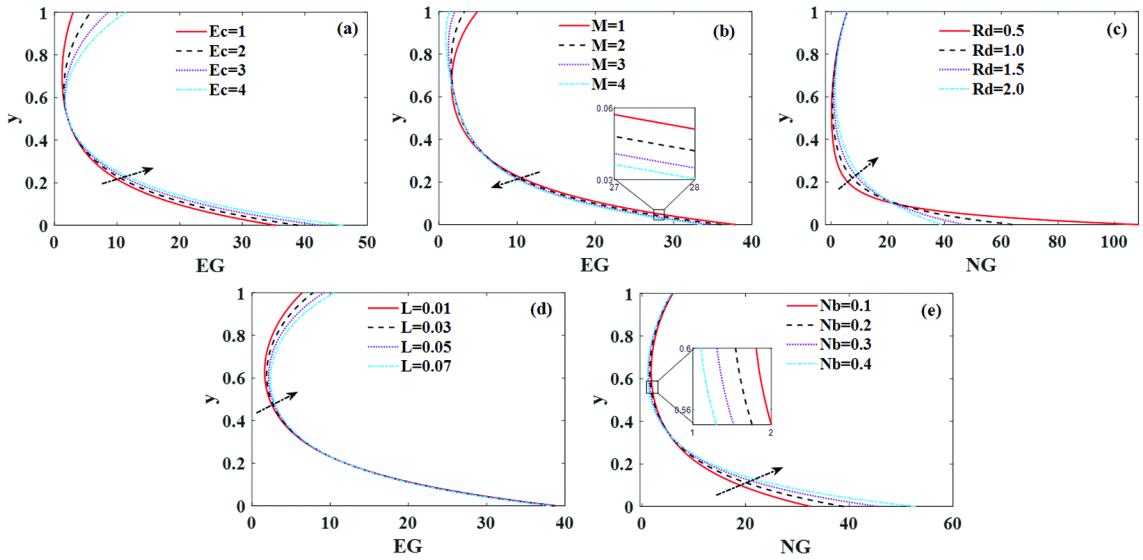

Fig. 9 — Response of entropy generation (NG) to (a) Ec, (b) M, (c) Rd, (d) L and (e) Nb

Heat and Mass Transfer

Table 2 provides discussions on the distributions of the Nusselt and Sherwood dimensionless values across hetrogeneous parameter conditions for We, Ec, Rd, M, Nt, Nb, γ_1, and Le at the lower and upper boundaries. A careful examination of the tabular measurements highlights the fact that the Nusselt number quickens with larger amounts of the viscous dissipation, Weissenberg number, radiation, thermophoresis, and Brownian motion parameters. In addition, Nu exposes a declining tendency when dealing with larger quantities of magnetic parameter, Lewis number, and chemical reaction parameter at the lower wall. For the upper wall, an increase in M, Rd, and γ_1 is observed to enhance the heat transfer rate. As with Carreau-Yasuda nanofluid, elevated values of We, Ec, Nt, Nb, and Le have a predisposition to decelerate the Nusselt number.

Simultaneously, an enhancement in the rate of mass transfer was observed with an increment in *M,*

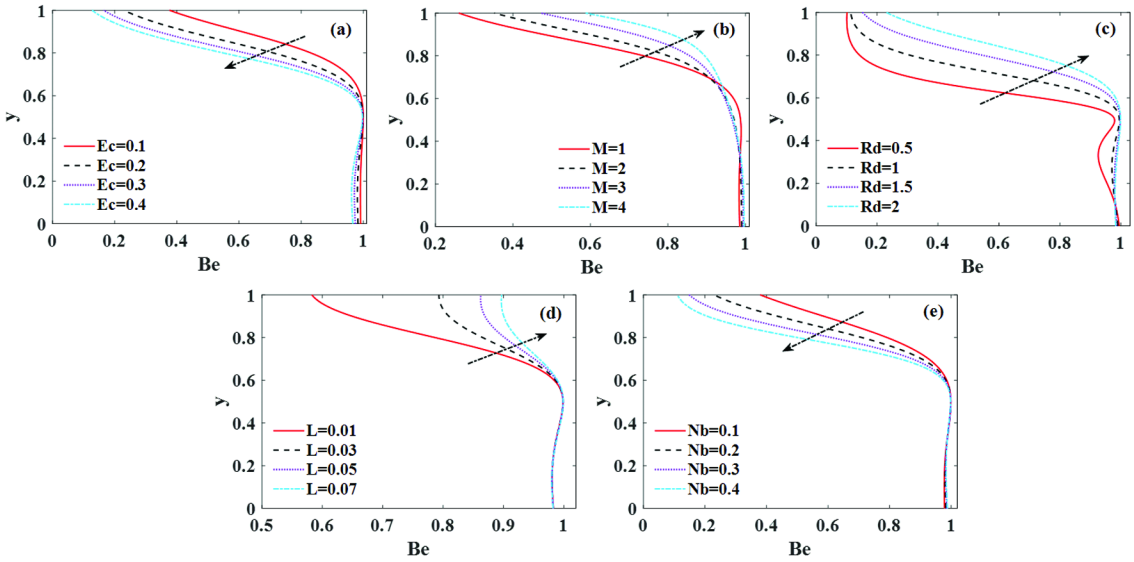

Fig. 10 — Response of Bejan number (Be) to (a) Ec, (b) M, (c) Rd, (d) L and (e) Nb (when Ec = 0.2)

Table 2 — At the boundaries y = 0 and y = 1, alterations in Sherwood and Nusselt numbers are examined for distinctive parameter configurations when $We = 3, n = 0.5, d = 2, t = \frac{\pi}{4}, = 0.1, Pr = 21, M = 0.3, Nb = 0.2, Le = 2.1, K_1 = 0.001, Rd = 2, _1 = 0.2, H = 1, Nt = 0.3, Ec = 2, \lambda_0 = 0.3, and\ \gamma_1 = 0.2.$

Parameters	Numerals	Nusselt		Sherwood	
		y = 0	y = 1	y = 0	y = 1
	1	11.05743150	0.50135390	-1.90622467	3.66032542
We	3	11.06538162	0.49699601	-1.90892284	3.66171599
	5	11.09312248	0.48024672	-1.91849170	3.66732931
	2	11.00405109	0.54080851	-1.88601942	3.64600880
M	4	10.91890245	0.58084341	-1.85770044	3.63434283
	6	10.86980955	0.59728484	-1.84247730	3.63086644
	0.1	10.81162430	0.61021165	-1.82550373	3.62997820
Ec	0.3	10.83828043	0.59831075	-1.83426530	3.63331423
	0.5	10.86494942	0.58640599	-1.84303139	3.63665138
	3	11.54682771	1.25494287	-1.06822790	3.61564654
Rd	4	12.41815101	2.18647141	-0.67498624	3.56087241
	5	13.46420931	3.22593965	-0.45252935	3.50956174
	0.5	17.84202498	0.20213248	-7.34167942	4.04668090
Nt	0.6	22.21588117	0.10936014	-12.0714779	4.21341017
	0.7	27.20535039	0.04173052	-18.4861683	4.36764791
	0.5	14.15626183	0.05754291	-0.98816228	3.27428635
Nb	0.6	15.10970796	0.00933135	-0.88148580	3.22417830
	0.7	16.03058231	-0.01799411	-0.80347754	3.18769726
	1	10.81829672	0.50020206	-1.43039798	6.97376162
γ_1	2	10.69826893	0.50218227	-1.17778497	9.66942454
	3	10.62645886	0.50307627	-1.03712572	11.7604589
	0.3	11.29261104	0.50101001	-2.10798811	2.52378545
Le	0.6	11.23718261	0.49970663	-2.06994216	2.73821346
	0.9	11.19117010	0.49876658	-2.03404079	2.94080397

Rd, Nt, γ_1, and *Le*. However, a dissimilar nature is noted for Sh concerning the enlargement of *Ec, We,* and *Nt* at the bottom boundary. At the upper wall, an increase in *We, Ec, Nt,* γ_1, and *Le* enhances the Sherwood number, while an increase in *M, Rd,* and *Nb* diminishes the mass transfer rate.

Conclusion

The investigation delved into how Brownian motion, Joule heat, thermophoresis, viscous dissipation, thermal radiation, and chemical reaction collectively influence a nanofluid in a channel subjected to MHD pulsatile flow. The chosen model for this study was the Carreau-Yasuda model,

a non-Newtonian model. The non-linear ODEs originated from dimensionless PDEs using the perturbation approach. The MATLAB bvp4c function is implemented for acquiring solutions to the problem. The significant findings pertaining to key variables are summarized below:

- The velocity of the nanofluid, whether steady or unsteady, experiences a reduction as n, d, and M increase, yet at the same time witnesses an ascent with the rise in the Weissenberg number.
- Enlarging the Brownian movement, thermophoresis parameter, and Eckert number corresponds to a rise in the steady temperature, while an escalation in Rd weakens θ_s.
- An upswing in *Nt, Le,* and γ_1 contributes to a decline in steady concentration, while hightened Browinian motion concurrently enhances ϕ_s.
- The heat transfer rate escalates in instances where We, Ec, Nb, and Nt are elevated, although it diminishes in the context of superior quantities of M, Rd, γ_1 and Le at wall y = 0.
- Intensifying M, γ_1, and Rd accelerates the Nussult number, while counterpart tendencies prevail for greater values of Ec, Nt, Le, and Nb at the top wall.
- An increment in Hartmann number, radiation parameter, Brownian motion, chemical reaction parameter, and Lewis number positively impacts the mass transfer rate, while a contradictory trait emerges in favor of uplifting Weissenberg number, Eckert number, and thermophoresis parameter at boundary y=0.
- Significant amplification in Sherwood number is evident upon escalation of Ec, We, γ_1, Nt, and Le at wall y = 1.
- Raising the Eckert number and Brownian motion parameter significantly intensifies NG while causing a diminution in Be.
- The expansion of radiation and diffusion parameters contributes to the promotion of the Bejan number and the generation of entropy.

Conflict of interest

The authors declare no conflict of interest.

References

1 Choi S U S & Eastman J A, Enhancing thermal conductivity of fluids with nanoparticles, *Am Soc Mech Eng Fluids Eng Div*, 231 (1995) 99.

2 Wang J, Yang X, Klemeš J J, Tian K, Ma T & Sunden B, A review on nanofluid stability: Preparation and application, *Renew Sust Energ Rev*, 188 (2023) 113854.

3 Michaelides E E, Brownian movement and thermophoresis of nanoparticles in liquids, *Int J Heat Mass Transf*, 81 (2015) 179.

4 Buongiorno J, Convective transport in nanofluids, *J Heat Transf*, 128 (2005) 240.

5 Mahmoodi M & Kandelousi S, Effects of thermophoresis and brownian motion on nanofluid heat transfer and entropy generation, *J Mol Liq*, 211 (2015) 15.

6 Rajkumar D, Reddy A S, Srinivas S & Jagadeshkumar K, Numerical investigation on pulsating hydromagnetic flow of chemically reactive micropolar nanofluid in a channel with brownian motion, thermophoresis and ohmic heating, *Int J Appl Comput Math*, 8 (2022) 119.

7 Vedavathi N, Dharmaiah G, Noeiaghdam S & Fernandez-Gamiz U, A chemical engineering application on hyperbolic tangent flow examination about sphere with brownian motion and thermophoresis effects using bvp5c, *Case Stud Therm Eng*, 40 (2022) 102491.

8 Anbuchezhian N, Srinivasan K, Chandrasekaran K & R Kandasamy, Thermophoresis and brownian motion effects on boundary layer flow of nanofluid in presence of thermal stratification due to solar energy, *Appl Math Mech*, 33 (2012) 765.

9 Mutuku W N & Makinde O D, Double stratification effects on heat and mass transfer in unsteady mhd nanofluid flow over a flat surface, *Asia Pac J Comput Eng*, 4 (2017) 1.

10 Madkhali H A, Ahmed M, Nawaz M, Alharbi S O, Alqahtani A S & Malik M Y, Computational study on the effects of brownian motion and thermophoresis on thermal performance of cross fluid with nanoparticles in the presence of ohmic and viscous dissipation in chemically reacting regime, *Comp Part Mech*, 11 (2024) 1301.

11 Khan M I, Alzahrani F, Hobiny A & Ali Z, Estimation of entropy generation in Carreau-Yasuda fluid flow using chemical reaction with activation energy, *J Mater Res Technol*, 9 (2020) 9951.

12 Qayyum M, Riaz M B & Afzal S, Analysis of blood flow of unsteady Carreau-Yasuda nanofluid with viscous dissipation and chemical reaction under variable magnetic field, *Heliyon*, 9 (2023) e16522.

13 Migtaa H A & Al-Khafajy D G S, Influence of heat transfer on magnetohydrodynamics oscillatory flow for Carreau-Yasuda fluid through a porous medium, *J Al-Qadisiyah Comput Sci Math*, 11 (2019) 76.

14 Dubey A, Vasu B, Bég O A & Gorla R S R, Finite element computation of magneto hemodynamic flow and heat transfer in a bifurcated artery with saccular aneurysm using the Carreau-Yasuda biorheological model, *Microvasc Res*, 138 (2021) 104221.

15 Kada B, Pasha A A, Asghar Z, Khan M W S, Aris I B & Shaikh M S, Carreau-Yasuda fluid flow generated via metachronal waves of cilia in a micro-channel, *Phys Fluids*, 35 (2023) 013110.

16 Ye Q, Zhang Y & Wei J, A comprehensive review of pulsating flow on heat transfer enhancement, *Appl Therm Eng*, 196 (2021) 117275.

17 Wang C Y, Pulsatile flow in a porous channel, *J Appl Mech*, 38 (1971) 553.

18 Radhakrishnamacharya G & Maiti M, Heat transfer to pulsatile flow in a porous channel, *Int J Heat Mass Transf*, 20 (1977) 171.

19 Wang X & Zhang N, Numerical analysis of heat transfer in pulsating turbulent flow in a pipe, *Int J Heat Mass Transf*, 48 (2005) 3957.
20 Bhargava R, Takhar H S, Rawat S, Beg T A A & Beg O A, Finite element solutions for non-Newtonian pulsatile flow in a non-Darcian porous medium conduit, *Nonlinear Anal Model*, 12 (2007) 317.
21 Kumar R & Prasad B, MHD pulsatile flow through a porous medium, *J Appl Fluid Mech*, 7 (2014) 63.
22 Adesanya S O, Falade J & Makinde O, Pulsating flow through vertical porous channel with viscous dissipation effect, *UPB Sci Bull D: Mech Eng*, 77 (2015) 25.
23 Govindarajulu K, Reddy A S & Chamkha A J, Entropy analysis on oscillating flow of third grade nanofluid in a channel with joule heating: A buongiorno model approach, *Eur Phys J Plus*, 138 (2023) 416.
24 Thamizharasan T & Reddy A S, Entropy generation on pulsatile hydromagnetic flow of Jeffrey nanofluid in a porous channel with Brownian motion, thermophoresis, and heat source/sink using Cattaneo-Christov heat flux, *Indian J Pure Appl Phys*, 60 (2022) 680.
25 Somasundaram R, Reddy A S, Srinivas S & Ramamohan T R, Impacts of brownian motion, thermophoresis and Ohmic heating on chemically reactive pulsatile mhd flow of couple stress nanofluid in a channel, *Indian J Pure Appl Phys*, 60 (2022) 354.
26 Josuva J & Reddy R H, Pulsatile hydromagnetic Carreau-Yasuda nanofluid flow in a nonlinearly radiated inclined porous channel with nonuniform heat source/sink: Entropy analysis, *Z Angew Math Mech*, 105 (2025) e70092.
27 Venkatesan G, Reddy A S, Srinivas S & Jagadeshkumar K, Pulsating hydromagnetic flow of chemically reactive Oldroyd-B nanofluid in a channel with Brownian motion, thermophoresis, and joule heating, *J Nanofluids*, 11 (2022) 604.
28 Kumar C, Srinivas S & Reddy A S, MHD pulsating flow of Casson nanofluid in a vertical porous space with thermal radiation and joule heating, *J Mech*, 36 (2020) 1.
29 Srinivas S, Challa K K, Badeti S & Kumar P B, Pulsatile powell-eyring nanofluid flow in a channel with inclined magnetic field and chemical reaction, *Eng Trans*, 71 (2023) 519.
30 Hayat T, Sajjad R, Abbas Z, Sajid M & Hendi A A, Radiation effects on MHD flow of Maxwell fluid in a channel with porous medium, *Int J Heat Mass Transf*, 54 (2011) 854.
31 Sheikholeslami M, Ganji D D, Javed M Y & Ellahi R, Effect of thermal radiation on magnetohydrodynamics nanofluid flow and heat transfer by means of two phase model, *J Magn Magn Mater*, 374 (2015) 36.
32 Ibrahim W & Negera M, Viscous dissipation effect on williamson nanofluid over stretching/shrinking wedge with thermal radiation and chemical reaction, *J Phys Commun*, 4 (2020) 045015.
33 Pal D & Talukdar B, Combined effects of joule heating and chemical reaction on unsteady magnetohydrodynamic mixed convection of a viscous dissipating fluid over a vertical plate in porous media with thermal radiation, *Math Comput Model*, 54 (2011) 3016.
34 Daniel Y S, Aziz Z A, Ismail Z & Salah F, Entropy analysis in electrical magnetohydrodynamic (MHD) flow of nanofluid with effects of thermal radiation, viscous dissipation, and chemical reaction, *Theor App Mech Lett*, 7 (2017) 235.
35 Balla C S & Naikoti K, Radiation effects on unsteady MHD convective heat and mass transfer past a vertical plate with chemical reaction and viscous dissipation, *Alex Eng J*, 54 (2015) 661.
36 Srinivas S & Muthuraj R, Effects of thermal radiation and space porosity on MHD mixed convection flow in a vertical channel using homotopy analysis method, *Commun Nonlinear Sci Numer Simul*, 15 (2010) 2098.